Phenolic resin derivatized TiO 2 -walnut shell carbon hybrid materials for solar photocatalytic phenol removal

Tao Li
Southwest Forestry University)
Shiping Zhou
Southwest Forestry University)
Fengchuan Li
Southwest Forestry University)
Huijuan Li
muzilihuijuan@163.com

Southwest Forestry University)

Research Article

Keywords: TiO2, walnut shell carbon, phenol-formaldehyde resin, phenol removal, Adsorption-photocatalysis synergistic effect

Posted Date: August 16th, 2023

DOI: https://doi.org/10.21203/rs.3.rs-3248600/v1

Additional Declarations: No competing interests reported.

Version of Record: A version of this preprint was published at Journal of Sol-Gel Science and Technology on April 9th, 2024. See the published version at https://doi.org/10.1007/s10971-024-06370-4.

Abstract

In this study, phenolic resin modified TiO_2 (PF/TiO_2), TiO_2/WSC (Walnut shell carbon) and PF/TiO_2/WSC hybrid composites were successfully synthesized by sol-gel method. The obtained TiO_2-based composites were characterized by XRD, SEM, FTIR and XPS techniques. The phase characterization results showed that TiO_2 phase is anatase in PF/TiO_2/WSC (300℃, 2h) composite material, also TiO_2 was uniformly loaded on the surface of the WSC to make the binding energy of Ti shift. Ti–O–C bonds are formed in the prepared TiO_2/WSC and PF/TiO_2/WSC (300℃, 2h) photocatalyst. When the catalyst dosage was 2.0 g/L, the initial phenol concentration was 80 mg/L, 10%PF/30%TiO_2/WSC composite showed the best activity and its degradation rate was 88.14% under sunlight for 150 min. The active centers of PF/TiO_2/WSC photocatalytic degradation of phenol were ·OH and $\cdot O_2^-$, and the photocatalytic degradation mechanism was proposed. The synergistic system of WSC adsorption and the superior photocatalytic performance of phenolic resin modified TiO_2 achieved high degradation efficiency of pollutants in water and provided a new idea for solar photocatalytic removal of pollutants.

1. Introduction

Since Fujishima reported the research method of photocatalytic water splitting to produce hydrogen in 1972 [1], the development of photocatalytic technology has become a research hotspot. The common photocatalysts include semiconductor metal oxides TiO_2 [2–5]. Compared with other photocatalysts, TiO_2 has high catalytic activity and chemical stability, and become one of the most widely used in nanoscale structure [6–8]. However, nano-powder is easy to agglomerate and deactivate in a high concentration environment, and nano-TiO_2 left in water may have potential cytotoxicity to organisms [9–11]. Thus, TiO_2 loaded on the carriers study is a hot point, and many materials are explored as TiO_2 support. Biomass carbon (BC), as a support for TiO_2, is the new type of adsorbent that has been used in the photodegradation of phenols pollutants in aqueous phase, which has been shown super phenol removal for adsorption-photocatalysis synergistic effect [12]. Srisasiwimon *et al.*[13] prepared TiO_2/lignin composite and found that the ratio of TiO_2 and lignin ratio 1:0.5 presented good characteristics and showed the highest photocatalytic activity under UV irradiation for 5 h. Kuncewicz *et al.*,[14] found that the C/TiO_2 composite photocatalyst synthesized by chromate had the photocatalytic activity of oxidizing 4-chlorophenol (4-CP).

Walnut shell carbon is cheap and wide range of sources, it can obtain a large specific surface area and a strong adsorption capacity for pollutants in water, but it is difficult to completely mineralize the adsorbed substances. Combining walnut shell carbon with TiO_2 to prepare TiO_2/walnut shell carbon composites can have superior properties with better adsorption and photocatalysis efficiency [15–17]. Although the TiO_2/walnut shell carbon composite system has a strong effect on removing pollutants in water, it is difficult to fix TiO_2 on the surface of the walnut shell carbon in the actual production process. As a widely used adhesive, phenolic resin can play an adhesive role in the solid loading process [18]. In addition, the

doping of phenolic resin can form a conjugated structure with Ti-O on the surface of TiO_2, resulting in electrons can transfer to the conduction band of TiO_2 and thereby enhance the responsiveness of TiO_2 to visible light and improve the photocatalytic efficiency of TiO_2 under natural sunlight.

In the present work, the phenolic resin-modified TiO_2/walnut shell carbon composite (PF/TiO_2/WSC) was prepared by sol-gel method. The obtained PF/TiO_2/WSC composite was used for phenol degradation under natural sunlight. The influence of calcined temperature, water sources and other causes for phenol degradation were explored. And also characterization of PF/TiO_2/WSC composite, such as XRD, SEM, FT-IR and XPS were used to characterize the obtained composites. A possible systematic effect mechanism for phenol removal was proposed.

2. Experimental contents and methods

2.1 Materials

Walnut shell was collected by market of Kunming in China. Tetra-n-butyl titanate ($C_{16}H_{36}O_4Ti$, 99.9%), Acetic acid (CH_3COOH, 99.5%), phenol (C_6H_6O 99%) were supplied by Shanghai Chemicals Ltd, China. And magnetic stirrer came from Ronnie ko (Shanghai) instrument co., LTD).

2.2 Preparation of PF/TiO_2 /WSC composites

2.2.1 Preparation of walnut shell carbon

The washed walnut shells were collected and washed thoroughly with deionized water for several times, and dried at 110 ℃ for 24 h. The dried waste walnut shell was pretreated in 100 mL 0.1 mol/L KOH aqueous solution under magnetic stirring at room temperature for 4 h. After that, the sample was dried in an oven at 110 ℃ for 24 h, and then the dried walnut shell was put into muffle furnace calcined at 700℃ for 2 h to prepare walnut shell carbon (WSC).

2.2.2 Synthesis of TiO_2/WSC

A series of TiO_2/WSC samples was prepared via the sol-gel method. In a typical synthesis to obtain TiO_2/WSC, 10 mL tetrabutyl titanate was added slowly to a solution containing 2 mL absolute ethanol and 6 mL acetic acid mixed solution, also with certain amount WSC under vigorous stirring for 10 min in a 250 mL beaker, the suspension was stirred until gelation. The obtained gel was aged for 24 h, dried at 110°C for 24 h, and then calcined in air at different temperatures for 2 h to obtain TiO_2 /WSC samples.

2.2.3 Synthesis of PF/TiO_2/WSC

To obtain PF/TiO_2/WSC, a certain amount of PF dissolved in water and was added to the obtained TiO_2 and WSC sol mixture, and also the same procedure (dried 110 ℃ for 24 h, calcined at different temperatures for 2h) was employed to produce the PF/30%TiO_2/WSC (designated as x% PF/30%TiO_2

/WSC, where x is the mass percentage of PF relative to 30%TiO_2/WSC, the mass of PF was 0.10 g and the mass of 30%TiO_2/WSC was 1.00 g).

2.3 Evaluation of photocatalytic activities for pollutant degradation

Phenol adsorption in the dark and the photodegradations were performed at 25 ºC. Under stirring, 0.2 g obtained photocatalyst was added in 100 mL phenol solution. The initial concentration of phenol was 80 mg/L. And the mixed solution was stirred in the dark for 30 min to achieve the adsorption-desorption balance, then the photocatalytic experiments were performed on sunny days between 11:00 and 14:00 during the September and October in Kunming, China (24 48’ N, 102 40’ E). The average intensity of sunlight striking the surface of the reaction solution was 0.700 kw/m^2 measured by a digital luxmeter. At specific time intervals, 2 mL of the solution was withdrawn from the system, centrifuged, and the concentration of the phenol was monitored using a UV-7200 spectrophotometer at λ = 270 nm. The degradation efficiencies of phenol were calculated by using Eq. (1).

Phenol conversion (%) = $(C_0\text{-}C_t) / C_0 \times 100\% = (A_0\text{-}A_t) / A_0 \times 100\%$ (1)

Where C_0 and A_0 are the concentration and absorbance of initial phenol solution, respectively,

While C_t and A_t are the concentration and absorbance of phenol at a certain irradiation or adsorption time, respectively.

2.4 Catalyst characterization

X-ray diffraction was examined by a horizontal Rigaku B/Max IIIB powder diffractometer with Cu Kα radiation and a power of 40 kV at 30 mA. Whereas the surface chemistry of catalysts were analyzed by Fourier transform infrared spectra (FT-IR) recorded on the Varian 640 spectrometer (USA) operating in the range of 400–4000 cm^{-1} with a resolution of 4 cm^{-1} and 32 scans/s, samples were ground with spectroscopic grade KBr. Scanning electron microscop (SEM) was tested by a Hitachi H-800 transmission electron microscope (Japan) for investigating the morphology of photocatalysts. The surface elements of catalysts were researched by X-ray photoelectron spectroscopy (XPS) using an ESCALAB 250Xi X-ray photoelectron spectrometer. The ultraviolet visible diffuse reflectance spectra were recorded on a Shimadzu UV 3600 spectrophotometer; the catalysts were examined at room temperature with wavelength from 200 nm to 700 nm.

2.5 Photo electrochemical measurements

The photo electrochemical properties including photocurrent response (PCR) of the obtained samples were investigated by CHI660 electrochemical workstation. In the standard three-electrode system, the samples film coated on stainless steel sheet, saturated calomel electrode (SCE) and platinum wires were used as working electrode, reference electrode and counter electrode, respectively. 0.1 mol/L Na_2SO_4

solution was used as the electrolyte solution. A 50 W Xenon lamp with 420 nm cutoff filter was applied as the visible light source and the measurements were conducted at room temperature.

3. Results and discussion

3.1 Sample characterization

3.1.1 XRD characterization

Fig.1 XRD patterns of the different composites (a) and 10%PF/30%TiO_2/WSC

calcined at different temperatures (b)

In order to verify the crystalline phase of the samples, XRD patterns of different samples and 10%PF/30%TiO_2/WSC calcined at different temperatures are provided in Fig. 1. As can be seen from the Fig.1a, the diffraction peak of walnut shell carbon is mainly located at 2θ =23.2° and 43.6°, which belong to the fat chain of hexagonal carbon, the microcrystals with irregular and disordered graphite structure and also walnut shell carbon has been partially graphitized. For the XRD patterns of TiO_2-based photocatalysts, the main diffraction peak is 2θ= 25.28°, 37.86°, 48.01°, 54.01° and 62.57° correspond to (101), (004), (200), (105) and (204) crystal planes of anatase TiO_2 (JCPDS No. 21–1272)[19]. After TiO_2 loaded on WSC to prepare TiO_2/WSC, it can be seen that the crystalline peak intensity of TiO_2 decrease, and also XRD spectra for 10%PF/TiO_2, the main diffraction peak of TiO_2 has shifted and became small, which indicates that the carbon atoms enter into the TiO_2 lattice after carbonization. And further loaded TiO_2 on the walnut carbon to get PF/TiO_2/WSC, reduces the crystalline peak intensity of TiO_2, indicating that the existence of walnut shell carbon promotes the dispersion of TiO_2 and further reduces the particle size of TiO_2. The XRD diffraction peaks of 10%PF/30%TiO_2/WSC composites calcined at different temperatures is showed in Fig.1b. It can be seen that TiO_2 and walnut shell carbon coexist characteristic diffraction peaks. And TiO_2 anatase phase diffraction peak intensity becomes sharp with increasing calcination temperature, indicating that TiO_2 crystalline phase is more complete, and no rutile phase TiO_2 diffraction peak is observed until the calcination temperature is 700 ℃, suggesting that the loading on the walnut shell carbon can stabilize the photocatalytic active anatase TiO_2 phase.

Table 1 shows the grain size of TiO_2 in different catalysts calculated by the Scherrer's equation: $D = K\lambda/\beta\cos\theta$, where D is the crystal size, K is the wavelength of the X-ray radiation (λ= 0.15406 nm), which is usually taken as 0.89, and β is the peak width at the half-maximum height of the sample. According to Scherrer equation, the average crystallite size of pure TiO_2, 10%PF/TiO_2 (300 ℃), 30%TiO_2/WSC (300 ℃) and 10%PF/30%TiO_2/WSC (300 ℃) is 8.21 nm, 7.12 nm, 5.80 and 4.02 nm, respectively, which shows that PF doping and loading on walnut carbon can reduce the agglomeration of TiO_2 effectively and decrease the crystal size. Also the average crystallite size increased with calcined temperature. 10%PF/30%TiO_2/WSC (300 ℃) has little crystallite size and thus promote its photocatalytic activity.

Table.1 The grain size of TiO_2 in different catalysts

Sample	TiO_2 grain size/nm
TiO_2 (300 ℃, 2 h)	8.21
10%PF /TiO_2 (300 ℃, 2 h)	7.17
30%TiO_2/WSC (300 ℃, 2 h)	5.80
10%PF/30%TiO_2/WSC (200 ℃, 2 h)	3.63
10%PF/30%TiO_2/WSC (300 ℃, 2 h)	4.02
10%PF/30%TiO_2/WSC (400 ℃, 2 h)	7.24
10%PF/30%TiO_2/WSC (600 ℃, 2 h)	9.96
10%PF/30%TiO_2/WSC (700 ℃, 2 h)	13.00

3.1.2 UV–Vis diffuse reflectance spectra analysis

Fig.2. Diffuse reflectance spectra of pure TiO_2 and TiO_2-based hybrid photocatalysts

The optical absorption properties of photocatalysts play an important role in evaluating its photo absorption ability. Fig.2 shows diffuse reflectance spectra of pure TiO_2, 10%PF/TiO_2 and 10%PF/30%TiO_2/WSC photocatalysts. Results show that strong absorption mainly occurred in UV-light (λ<350 nm) and the weak absorption happened in visible region for pure TiO_2. When TiO_2 was modified with PF, 10%PF/TiO_2 turned pure orange. The complex formed exhibited strong absorption in the visible light region compared to pure TiO_2. Also 10%PF/30%TiO_2/WSC has better visible adsorption than pure TiO_2 [20-21]. According to the K-M equation Eg=1240/λ_0 (where is the Eg band gap width, λ_0 is the light absorption edge), the band gap width of 10%PF/30%TiO_2/WSC is 2.40 eV the band gap width of 10%PF/TiO_2 is 2.62 eV and the band gap width of TiO_2 is 2.93 eV. It indicates that pure TiO_2 has the worst response to visible light, while the addition of PF can generate conjugated structure with TiO_2, leading to electron transition to TiO_2 conduction band by virtue of conjugated system, indicating that PF modified contribution is responsible for decreasing in the energy band gap [22]. In addition, walnut shell carbon in composite materials can also provide a channel for electron transport, thus reducing the electron-hole recombination rate and enhancing the effect of TiO_2 on visible light [23]. Therefore, 10%PF/30%TiO_2/WSC composite has the best response to visible light, which indicates that the composite material can improve the solar photocatalysis by enhancing the response ability of TiO_2 to visible light.

3.1.3 Electrochemical characterization of photocatalysts

Fig. 3 shows *i-t* curves of the steel electrode prepared by two different catalysts under natural sunlight irradiation, in which the catalyst can absorb light within 100-200 s and 300-400 s. It suggests that different photocatalysts have different responses to visible light, resulting in different current values [24]. Photogenerated electrons are indeed generated and captured by the electrochemical workstation, thus detected the current. As can be seen from the Fig.3, the current at the switching point of the sunlight irradiation, i.e., 100 s, 200 s and 300 s, has an obvious jump change, and the order of current intensity at the switching stage is 10%PF/30%TiO_2/WSC > 10%PF/TiO_2>TiO_2. In addition, it can be seen from the UV-vis spectra data that 10%PF/30%TiO_2/WSC composite material has a higher response ability to visible light than TiO_2, so when the two catalysts are irradiated by the same visible light, the amount of current generated is different. In summary, electrochemical characterization further proves that the prepared catalysts can generate photogenerated electrons under light conditions, and the rate of electron generation is fast.

Fig.3 Electrochemical i-t curves of different catalysts

3.1.4 SEM characterization of photocatalyst .

Fig. 4 SEM images of WSC (a) ,30%TiO_2/WSC b and 10%PF/30%TiO_2/WSC (c) composites

SEM was used to observe the morphology structure of WSC, 30%TiO_2/WSC and 10%PF/30%TiO_2/WSC composites, which showed in Fig.4. It was obvious that many dense pores with regular size produced, the well-interconnected porous structure contained much more channels, which could expose more adsorption sites and easy transfer the pollutant molecules, also can afford a good support for TiO_2 loading. For 30%TiO_2/WSC, it can be seen that obvious little particles spread over the surface, and also pore and interlayer structure appeared, suggesting that TiO_2 is dispersed on the surface of walnut shell carbon. After modified with PF, the exposed pores on the composite surface are less, while the surface is more rough and the interlayer structure has not changed significantly, indicating that PF coating effect leads to the reduction of pores exposed on the surface, and the interlayer structure and rough surface can guarantee the 10%PF/30%TiO_2/WSC retain good adsorption and photocatalysis performance.

3.1.5 FT-IR spectra of different photocatalysts

FT-IR spectra of pure TiO_2 and TiO_2-based photocatalysts are presented in Fig.5. For pure PF, peak around 3469 cm^{-1} is ascribed to O-H bonding, the peaks present at about 3047 cm^{-1} correspond to C-H and -CH_2- stretching vibration modes, and peak at 1683 and 1443 cm^{-1} is attributed to the $\nu_{C=C}$ and ν_{C-H} vibration of aromatic ring; Peak at 1132 cm^{-1} is attributed to ν_{C-O} stretching vibration of resorcinol and methylol groups [25]. For WSC, the broad absorption peak at 1591 cm^{-1}, 1444 cm^{-1} and 1041 cm^{-1} were attributed to the deformation vibration of hydroxyl groups, on the surface of the composites and the water molecules adsorbed on the surface [26-27], C=C vibration adsorption peak (Aditya Chauhan *et al*; 2020) and C-C bands adsorption. For pure TiO_2, 3469 cm^{-1} was attributed to the stretching of O-H, and the

absorption peaks between 400 and 800 cm^{-1} were assigned to the Ti-O stretching and Ti-O-Ti bending, which are characteristic of the anatase TiO_2. As the binary composites, 10%PF/TiO_2 and 30%TiO_2/WSC, TiO_2 and WSC FT-IR peak were obviously appeared. And for ternary composites-10%PF/30%TiO_2/WSC, the TiO_2 and other organic species FT-IR vibration peak make smaller than pure TiO_2, which mightbe caused by TiO_2 dispersed on the walnut shell carbon and decreased its peak intensity. In addition to TiO_2 loading on WSC or PF modified, bands at 453 cm^{-1} became sharp, based on reported literature, the respective absorption band for 10%PF/30%TiO_2/WSC indicates the formation of Ti-O-C bond in the TiO_2-hybrid composite samples which can change the optical and charge transfer properties, also Ti-O-C vibration bond appeared which can be thought that carbon atom can doped into TiO_2 molecular structure [28].

Fig.5 FT-IR spectra of different photocatalysts

3.1.6 XPS characterization

Fig.6 (a) XPS survey spectra of TiO_2 and 10%PF/30%TiO_2/WSC, (b) XPS spectra of C1s (TiO_2), (c) XPS spectra of C1s (10%PF/30%TiO_2/WSC), (d) XPS spectra of Ti2p (TiO_2), (e) XPS spectra of Ti2p (10%PF/30%TiO_2/WSC), (f) XPS spectra of O1s (TiO_2), (g) XPS spectra of O1s (10%PF/30%TiO_2/WSC)

In order to analyze the chemical composition of the pure TiO_2 and 10%PF/30%TiO_2/WSC and to identify the chemical state of C, O and Ti elements, the XPS spectrum of the composites was employed (Fig.6). XPS survey spectra of TiO_2 and 10%PF/30%TiO_2/WSC (see in Fig.6a) showed that it has C, O and Ti elements coexisted on the surface of the two photocatalysts. The C1s XPS spectra of pure TiO_2 can be identified into three peaks with binding energy of 284.76 eV, 286.13 eV and 288.54 eV (Fig. 6b). Also, the peak at 284.76 eV is derived from the C=C bond of graphene, the peak at 286.13 eV is due to the C-O or C-N group, the peak at 288.54 eV is related to the O-C=O bond, and the peaks shift higher banding energy for 10%PF/30%TiO_2/WSC. As can be seen from the Table 2, PF modification and the walnut shell carbon loading gave a 6% increase in C=C content on the surface of the composite material, and a sharp increase in -OH content on the surface. Meanwhile, the peak position of the composite material has a certain deviation compared with pure TiO_2 [29-31]. Which indicates that the chemical environment of Ti in TiO_2 loaded 10%PF/30%TiO_2/WSC is different from that of pure TiO_2, and is probably due to the strong interaction between TiO_2 nanoparticles and the 10%PF/30%TiO_2/WSC and the formation of Ti–O–C bond [32], which also confirmed by our FTIR results (see Fig.5).

As a result, the electron density around Ti changes and the binding energy shifts. As can be seen from Table 2, the atomic mass ratio of C and Ti of 10%PF/30%TiO_2/WSC composites is similar to that pure TiO_2, but the mass ratio of oxygen is different to some extent. As there are oxygen-containing functional groups in both the modified walnut shell carbon and PF, the mass ratio of oxygen in the ternary composites exceeds that of Ti. XPS data analysis showed that PF modified TiO_2 and supported on walnut shell carbon, the content of hydroxyl group on the surface of TiO_2 increased, and the surface

hydroxyl group could be converted into photocatalytic active center ·OH under natural sunlight. In summary, 10%PF/30%TiO_2/WSC composites has more C=C bonds and surface hydroxyl groups, which can promote photogenerated electrons transferred from TiO_2 to walnut shell carbon efficiency, increase the separation of photogenerated electrons and holes, and also more active sites. Adding to its superior adsorption performance for walnut shell carbon, 10%PF/30%TiO_2/WSC composites deserved higher phenol removal efficiency.

Table.2 The combined state and relative atomic percentage of each element of 10%PF/30%TiO_2/WSC

Line	Binding energy / eV		Structure	Atomic percentage / %	
	TiO_2	10%PF/30%TiO_2/WSC		TiO_2	10%PF/30%TiO_2/WSC
C-1s	284.76	284.75	C-(C ,H); C=C	58.24	61.63
	286.13	286.16	C- (O, N)	24.60	25.27
	288.54	288.58	O-C=O	17.16	13.10
Ti-2p	458.77	459.71	Ti-$2p_{3/2}$	49.40	49.46
	464.56	465.51	Ti-$2p_{1/2}$	50.60	50.54
O-1s	529.84	530.89	Ti-O	60.20	42.71
	530.89	532.26	surface O-H	39.80	57.29

3.2 Study on photocatalytic performance of TiO_2-based catalysts

3.2.1 Photocatalytic phenol performance of various TiO_2-based catalysts

The adsorption-photocatalytic efficiency of the prepared catalysts was evaluated by 80 mg/L phenol aqueous solution. The phenol degradation efficiency (%) of the composites plotted against the reaction time (t) of pure TiO_2, 30%TiO_2/WSC, 10%PF/TiO_2, WSC and 10%PF/30%TiO_2/WSC composites is shown in Fig.7. Results show that phenol degradation is given in the two stage-processes: (i) the dark adsorption process and (ii) the sunlight-induced photocatalytic degradation process. For the first 30min, phenol removal efficiency on the TiO_2-based catalysts differs from each other. TiO_2 and PF/TiO_2 had almost no phenol adsorption efficiency, and when supported on WSC, the phenol adsorption increased to nearly 43%. The net phenol removal during the degradation process by TiO_2, 10%PF/TiO_2, WSC, 30%TiO_2/WSC and 10%PF/30%TiO_2/WSC was 18.56%, 35.82%, 68.01%, 78.97% and 93.91%, respectively. It is clearly demonstrated that TiO_2 loaded on WSC and PF modified could greatly increased TiO_2 photocatalysis efficiency.

In addition, due to the synergistic effect of adsorption and photocatalysis process, phenol adsorbed on the catalyst surface is degraded when exposed to sunlight, providing a new adsorption site. This synergistic effect can continue in the photocatalytic process, and the phenol removal rate of 10%PF/30%TiO_2/WSC composite is higher than other obtained composites.

Fig.7 Combined adsorptive and photocatalytic phenol over different photocatalysts.

3.2.2 Effect of 10%PF/30%TiO_2/WSC calcination temperature on phenol removal

Fig. 8 Effect of 10%PF/30%/TiO_2/WSC calcination temperature on phenol removal

Fig.8 shows the activity curve of photocatalytic degradation over 10%PF/30%TiO_2/WSC calcined at different temperatures. It can be seen from the Fig.8 that phenol degradation rates of 10%PF/30%TiO_2/WSC increased rapidly with time and then gradually stabilized. The phenol degradation rate of 10%PF/30%TiO_2/WSC calcined at 300 ℃ was higher than that of other calcined temperatures. Further increasing the temperature would not only transform TiO_2 from anatase to rutile phase, but also lead to PF carbonization, thus reducing the response ability of photocatalyst to sunlight. In addition, there is a synergistic effect of adsorption and photocatalysis in the 10%PF/30%TiO_2/WSC composite material. If the response ability to visible light is reduced, the phenol adsorbed on the surface of walnut shell carbon cannot be degraded in time, thus the purpose of reproducing active sites for walnut shell carbon cannot be achieved. Therefore, the roasting temperature of 10%PF/30%TiO_2/WSC composites was selected as 300℃. In addition, compared with other photo-adsorption catalysts (in Table.3), the catalytic performance of 10%PF/30%TiO_2/WSC is promising and super efficiency for phenol degradation.

Table. 3 Comparison of 10%PF/30%TiO_2/WSC with other catalysts for phenol removal.

Catalyst	C_{Cat} (g/L)	Time (min)	Phenol (ppm)	Conversion amount (mg /g)	References
TiO_2 /STARBON-800®	0.2	840	50	13.25	[33]
TiO_2 /Fe_2TiO_5 /Fe_2O_3	0.05	60	10	20.0	[34]
α-Fe_2O_3/TiO_2	0.02	60	10	50.0	[35]
TiO_2/SWP700	0.2	240	50	8.40	[36]
CM-n-TiO_2	0.1	300	60	25.8	[37]
10%PF /30%TiO_2/WSC	0.2	150	80	35.26	This study

3.2.3 Effect phenol removal efficiency on water sources over 10%PF/30%TiO_2/WSC

To explore the phenol degradation ability of 10%PF/30%TiO_2/WSC composite material in different water sources, including tap water and the real water samples of nearby rivers ("Dianchi Lake," Yunnan, China) were collected,. As can be seen from the Fig.9, when the reaction lasted for 30 min, the solution prepared by deionized water showed the higher removal efficiency than the other two water sources, and the difference gradually little as the reaction time went on. This is because both water sources contain small amounts of inorganic ion interfering substances(The ion content is shown in Table 4).At the beginning of the reaction, the walnut shell carbon adsorbed phenol and also other substances, decreased the phenol adsorption. For the reaction time increased, the degradation rate of phenol solution in two natural water bodies is gradually close to that of deionized water solution. At 150 min, the degradation rate of phenol solution in tap water reached 81.58%. However, Dianchi Lake water contains aquatic organisms, industrial and agricultural wastewater and domestic sewage, the water composition is relatively complex, the degradation rate is 80.99%, slightly lower than others. However, compared with phenol degradation rate in the three water sources, the little difference is less than 8%, indicating that the prepared 10%PF/30%/TiO_2/WSC has the ability to degrade pollutants in natural water.

Fig. 9 The influence of water source on the degradation of phenol by 10%PF/30%TiO_2/WSC

Tab. 4 Common chemical composition content in tap water, distilled water and Dian Lake water

Water source	Ca^{2+}/mg/L	Mg^{2+}/mg/L	Cl^-/mg/L	PO_4^{3-}/mg/L	Fe^{2+}/mg/L
Deionized water	0.001	0.001	0.001	0.001	0.001
Tap water	47.00	15.00	0.35	0.20	0.30
Dianchi Lake	41.30	37.65	0.74	0.46	1.58

Notes: All ion contents were determined by ourselves

Ca^{2+} Mg^{2+}: EDTA Titration method; Cl^-: Potentiometric titration method

PO_4^{3-}:Molybdenum blue colorimetric method; Fe^{2+}:Sulfosalicylic acid spectrophotometric method

3.2.4 Trapping experiments over the optimum 10%PF/30%/TiO_2/WSC composite

To understand the possible reaction mechanism for the photodegradation of phenol over the 10%PF/30%/TiO_2/WSC composite, free radical detection of photocatalytic activity of 10%PF/30%/TiO_2/WSC with different scavenges under solar light irradiation. In this investigation, benzoquinone, t-BuOH, KI, and EDTA were used as $\cdot O_2^-$, hydroxyl radical (•OH) and hole (h^+), scavengers, respectively. And the results are shown in Figure 10. It can be seen that the addition of benzoquinone, as $\cdot O_2^-$ scavenger, greatly decreased the photocatalytic efficiency, and the degradation ability of phenol with the addition of several scavengers is benzoquinone < tert-butanol (TBA) < potassium iodide (KI) < EDTA, which suggests that the $\cdot O_2^-$ plays the key role in the phenol photocatalytic degradation, and is the

reaction active center. And in normal knowledge, the photo-generated electrons do not participate in the degradation process, however, they can combine with oxygen to produce the active center $\cdot O_2^-$, thus promote the phenol degradation. And also the adding the potassium iodide and EDTA solution decrease the phenol removal little compared with original phenol solution, it seemed that the h^+ did not the reaction radicals. PF/TiO_2 loaded on the surface of WSC, and WSC has super electric conduction ability which can exceed the generated e^- by TiO_2 transfer to react with O_2, thus obtain $\cdot O_2^-$, and then increased the phenol removal by 10%PF/30%/TiO_2/WSC.

Fig. 10 Trapping experiments over 10%PF/30%/TiO_2/WSC for phenol degradation

3.2.5 Liquid UV characterization of phenol catalyzed by 10%PF/30%TiO_2/WSC

Fig. 11 UV-visible spectral changes of phenol solution as a function of reaction time

Phenol degradation process over 10%PF/30%TiO_2/WSC is recorded by liquid UV characterization and showed in Fig.11. It shows obviously that the phenol solution had strong absorption peaks at 210 nm and 269 nm. With the process of reaction, the two peak intensity decreased rapidly and tended to flat, indicating that the concentration of phenol in the solution decreased gradually with reaction time, and phenol was basically completely adsorbed on walnut shell carbon when the adsorption time reached 60 min. After that, it can be seen from Fig.11 that two new absorption peaks is generated at 220 nm and 240 nm, indicating that two new substances were generated in the adsorption-photocatalytic process. The intermediate products were contributed to be butenedioic acid (220 nm) and para-benzoquinone from the absorption peak at 240 nm. It indicated that phenol removal process contained phenol adsorption and photocatalytic conversion to CO_2, H_2O and other intermediates.

3.2.6 Phenol adsorption-photodegradation mechanism over 10%PF/30%/TiO_2/WSC

From the results of the structure characterizations and the natural sunlight photocatalytic activity of the prepared 10%PF/30%TiO_2/WSC, a possible synergistic effect between TiO_2 and WSC on the enhancement of photocatalytic activity is proposed (shown in Fig.12). Firstly walnut shell carbon has porous structure, large pore volume and large surface area, has a strong adsorption performance, provides pollutants enrichment effect for TiO_2 photocatalysis, and provides channels for TiO_2 electron transport, reducing the electron-hole recombination rate. The adsorption of phenol molecules and intermediates on WSC can provide more opportunities for photocatalyst to contact with phenol molecular; this allows further degradation on PF/TiO_2. Second, phenolic resin, as the adhesive and carbon doping substance, plays a fixed connection role in the composite material, and the phenolic hydroxyl group of PF can combine with the Ti-OH on the surface of TiO_2 to form conjugated system. Also, carbon doping is found for the presence of the Ti–O–C bonds found in FTIR and XPS spectra, carbon doping would introduce a mid band-gap state close to the TiO_2 valence bond, and also can increase phenol removal efficiency significantly. And also Ti-O-C structure appeared enhancing the response ability of TiO_2 to

visible light. When the composite photocatalyst irradiated by the natural sunlight, photo generated electron (e^-) and hole (h^+) are produced, PF modified TiO_2 can increase light adsorption and also can promote the drift away of electrons by transferring to WSC, which has good electron conductivity. Also photogenerated holes (h^+) and electrons combine water and dissolved oxygen in water to generate superoxide free radicals ($\cdot O_2^-$) and hydroxyl free radicals (·OH). These two free radicals can oxidize phenol into para-benzoquinone, and finally mineralize into small molecules H_2O and CO_2. The synergistic effect between TiO_2 photocatalytic efficiency and WSC adsorption on the phenol removal is coexisted.

Fig.12 Mechanism model of composite photocatalyst degradation of phenol

4. Conclusions

In the present work, phenolic resin modified TiO_2 loaded on porous WSC has been successfully prepared by sol-gel method, and then 10%PF/30%TiO_2/WSC composite materials were prepared by sol-gel method. The structure, surface morphology and surface element chemical states have been investigated. TiO_2 loaded on WSC and modified by PF had three main advantages:

1) The layered structure and pores of walnut shell carbon were retained in the composite, and TiO_2 dispersed evenly on the surface of walnut shell carbon, and decreased the crystallize size of TiO_2 sharply, which was beneficial for the adsorption of pollutants. In addition, the black carbon surface and PF modified was conductive to enhancing the utilization rate of light.

2) Ti–O–C bonds are formed in the prepared 10%PF/30%TiO_2/WSC photocatalyst. The carbon-doping source can decrease the band gap of TiO_2, improving the photocatalytic activity. And a large number of active free radicals (h^+, ·OH, $\cdot O_2^-$) effectively improved the oxidation ability, among them $\cdot O_2^-$ was more effective than others.

3) WSC can provide efficient transfer of charge and adsorbed reacting species, which can transfer the photoelectron and avoid photoelectron and holes combined, enhance the separation efficiency of photo-generated carriers effectively, and improve the photocatalysis ability.

Declarations

Acknowledgement:

The present study was supported by the Joint Project of Basic Agricultural Research Fund of Yunnan Province (2018FG001-051) and Open fund of Key Laboratory of State Forestry and Grassland Administration on Highly-Efficient Utilization of Forestry Biomass Resources in Southwest China (2022-KF06).

References

1. Fujishima A and Honda K 1972 *Nat*. **238** 37
2. Penboon L, Khrueakham A and Sairiam S 2019 *Water Sci. Technol*. **79** 958
3. Li X, Liu J J, Feng J, Wei T, Zhou Z X, Ma J et al 2023 *J. Hazard. Mat*. **445** 130400
4. Zhang W X, Yu Y, Huang R T and Shi X Y 2021 *ACS Appli. Mater. & Interf.* **13** 40571
5. Kong X Q, Li J Y, Yang C W, Tang Q and Wang D 2020 *Sep. Purif. Technol.* **248** 116924
6. Fagan R, McCormack D E, Dionysiou D D and Pillai S C 2016 *Mater. Sci. Semicond. Process.* **42** 2
7. Veljko R, Aleksandar D, Rada D P, Ovidiu E, Spyridon Z, Miodrag M et al 2020 *Appl. Mater. & Interf.* **12** 33058
8. Nabi G, Majid A, Riaz A, Alharbi T, Kamran M A and Al-Habardi M 2021 *Inorg. Chem. Commun*. **29** 108618
9. Pearson A, Jani H, Kalantar-zadeh K, Bhargava S K and Bansal V 2021 *Langmuir* **27** 6661
10. Le T T, Akhtar M S, Park D M, Lee J C and Yang O 2012 *Appl. Catal. B -Environ.* **111** 397
11. Jawad A H and Nawi M A 2012 *Reac. Kinet. Mech. Cat.* **106** 49
12. Ali S, Li Z J, Chen S Y, Zada A, Khan I, Ali W et al 2019 *Catal.Today* **335** 557
13. Srisasiwimon N, Chuangchote S, Laosiripojana N and Sagawa T 2018 *Sus. Chem. Eng.* **6** 13968
14. Kuncewicz J, ZaBek P, Stochel G, Stasicka Z and Macyk W 2011 *Catal. Today* **161** 78
15. Mountassir E, Mouchtari E, Daou C, Rafqah S, Najjar F and Anane H 2019 *J. Photochem. & Photobio. A: Chem.* 112183
16. Ahmed M A, Li M, Sanjrani M A, Abdelaal S A A, Norville B and Zhan Z W et al 2020 *ACS Omega* **5** 13630
17. Shi J, Huang W Y, Zhu H X, Xiong J H, Bei H T and Wang S F 2022 *ACS Omega* **7** 12158
18. Santhana P, Venkatesan N K and Adhinarayana K 2012 *J. Appl. Polym. Sci.* **69** 1483
19. Wang T, Meng Z F, Hua J, Jiang H, Sun X X and Jiang L C 2021 *Chemosphere* **263** 128106
20. Colmenares J C, Varma R S and Lisowski P 2016 *Green Chem.* **18** 5736
21. Srikanth B, Goutham R, Badri R, Ramprasath A, Gopinath K and Sankaranarayanan A 2017 *Environ. Manage.* **200** 60
22. Chen L J, Chen F, Shi Y F and Zhang J L 2012 *J. Phys. Chem. C.* **116** 8579
23. Fu M M, Mo C H, Li H, Zhang Y N, Huang W X and Wong M H 2019 *J. Clean. Prod.* **236** 117637
24. Guo F, Liu J M, Zhang W G, Yu Z B, Liu Y M and Liang W 2019 *Vacuum* **165** 223
25. Zhang X D, Wang J, Xiao B B, Pu Y J, Yang Y C, Geng J S et al 2022 *Appl. Catal. B: Environ.* **315** 121525
26. Silvestri S, Gonçalves M G, Veiga P A S, Matos T T S, Peralta Z Z and Mangrich S 2019 *Environ. Chem. Eng.* **2** 102879
27. Wang R Z, Huang D L, Liu Y G, Zhang C and Xu P 2019 *J. Haz. Mat.* **384** 121470

28. Fazal T, Razzaq A, Javed F, Hafeez A, Rashid N and Rehman F 2020 *J. Hazard. Mater* **390** 121623
29. Tsaneva V N, Kwapinski W, Teng X B A and Glowacki B A 2014 *Carbon* **80** 617
30. Elmouwahidi A, Bailón-García E, Pérez-Cadenas A F, Maldonado-Hódar F and Carrasco-Marín F 2017 *Electrochim. Acta* **229** 219
31. Lu L L, Shan R, Shi Y Y, Wang S X and Yuan H R 2019 *Chemosphere* **222** 391
32. Cong Y, Li X K, Qin Y, Dong Z J, Yuan G M and Cui Z G 2011 *Appl. Catal. B-Environ.* **107** 128
33. Colmenares J C, Lisowski P, Mašek O, Lisowski W, Lisovytskiy D and Grzonka J 2018 *Chem. Cat. Chem.* **10** 3469
34. Deng Y X, Xing M Y and Zhang J L 2017 *Appl. Catal. B-Environ.* **221** 157
35. Cong Y Q, Li Z, Zhang Y, Wang Q and Xu Q 2012 *Chem. Eng. J.* **191** 356
36. Lisowski P, Colmenares J C, Masek O, Lisowski W, Lisovytskiy Dand Kami-skaet 2017 *Sus. Chem. Eng.* **5** 6274
37. Shaban Y A, Sayed M A E, Maradny A A E, Farawati R K A and Zobidi M I A 2013 *Chemosphere* **91** 307

Figures

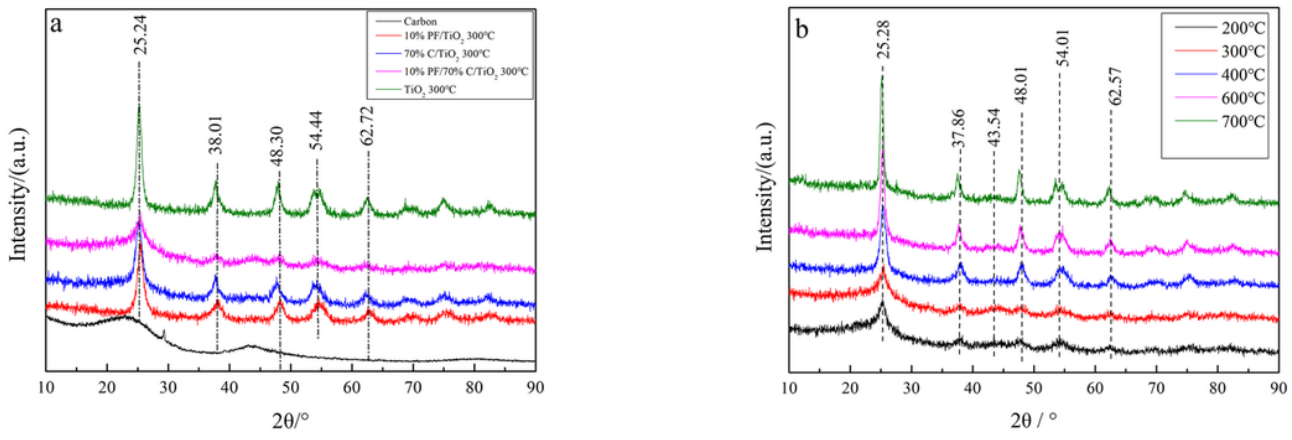

Figure 1

XRD patterns of the different composites (a) and 10%PF/30%TiO_2/WSC

calcined at different temperatures (b)

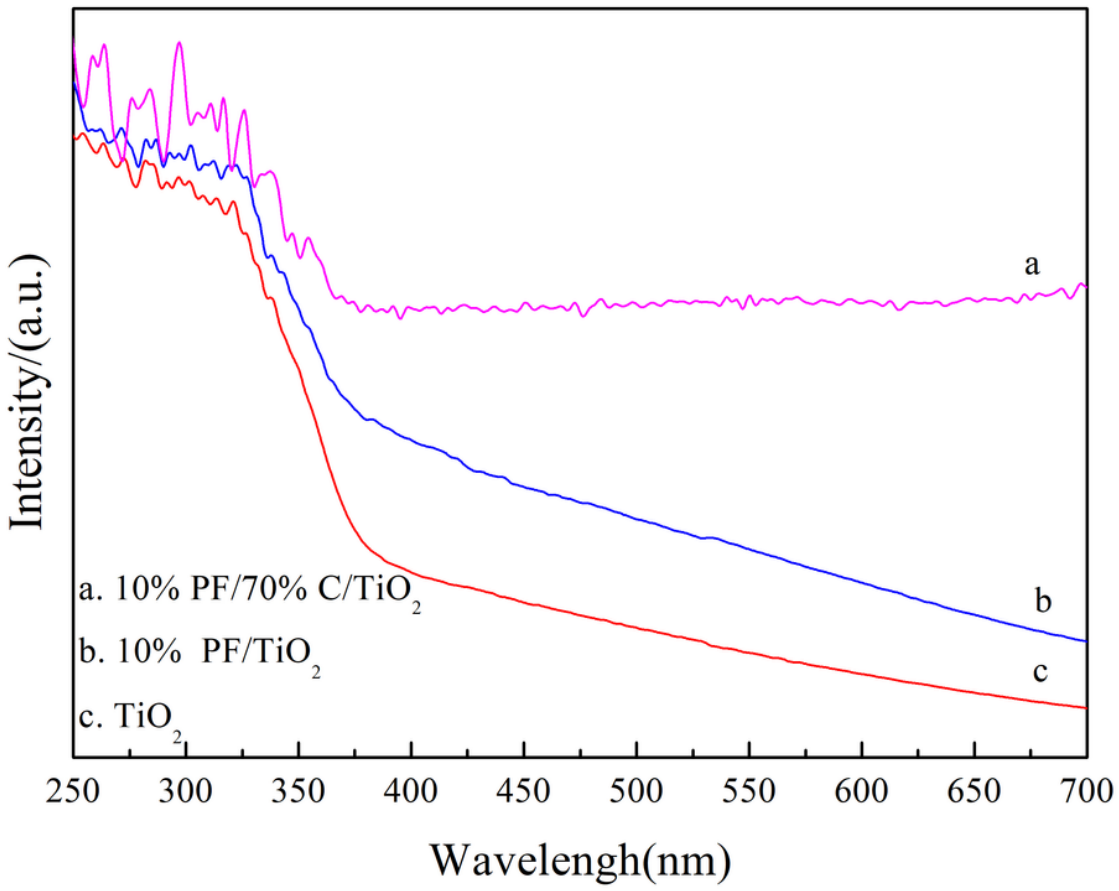

Figure 2

Diffuse reflectance spectra of pure TiO_2 and TiO_2-based hybrid photocatalysts

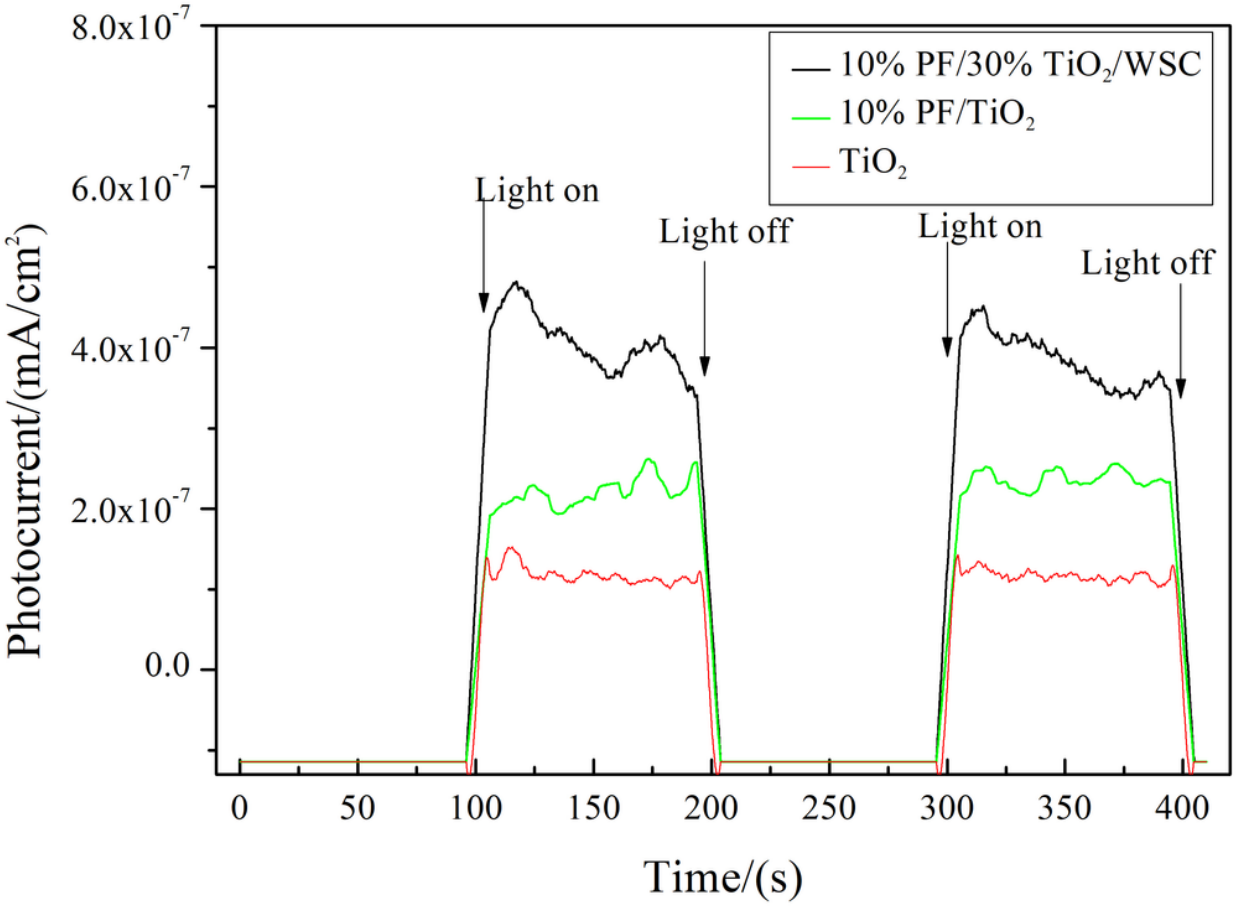

Figure 3

Electrochemical i-t curves of different catalysts

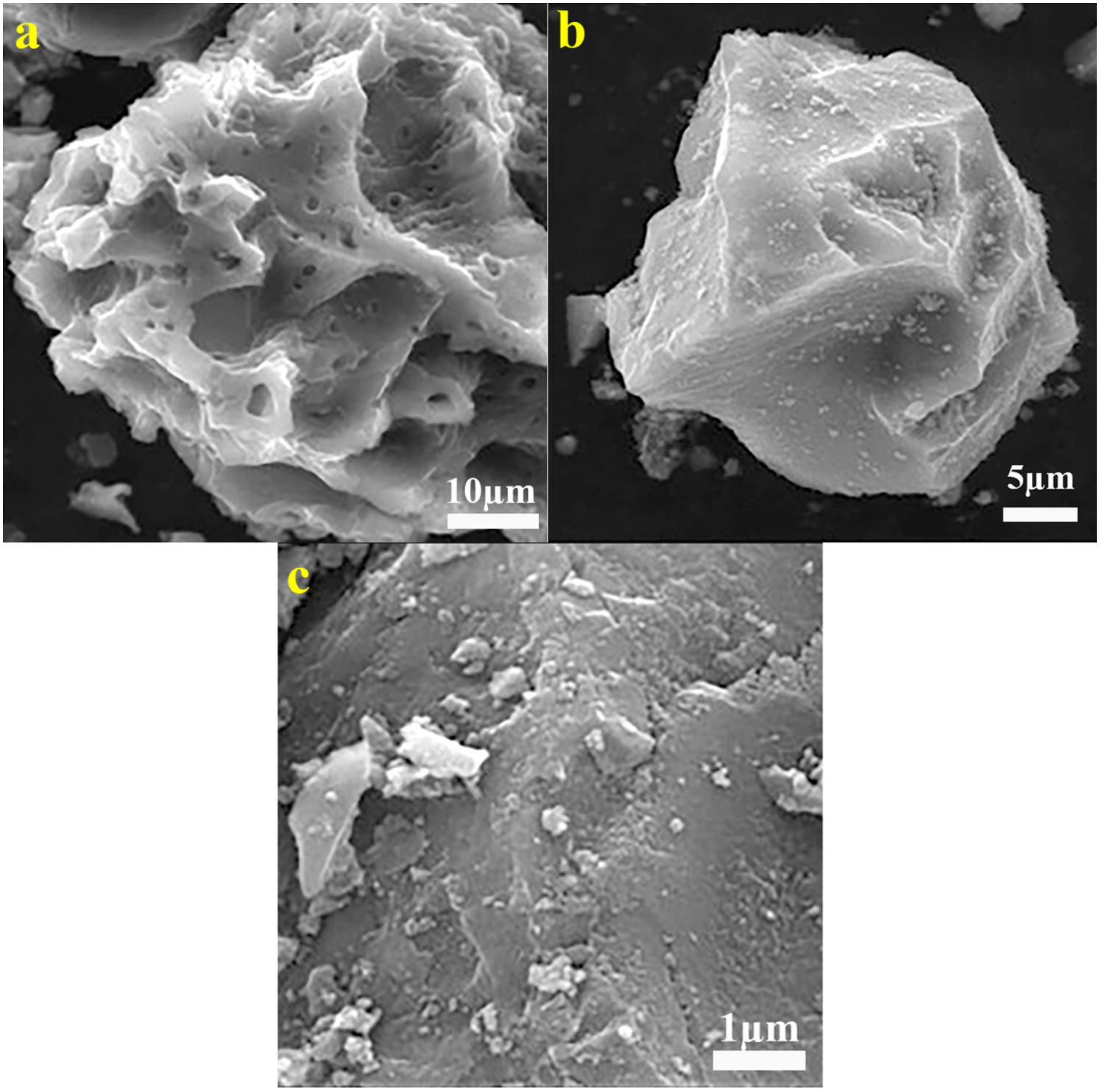

Figure 4

Legend not included with this version.

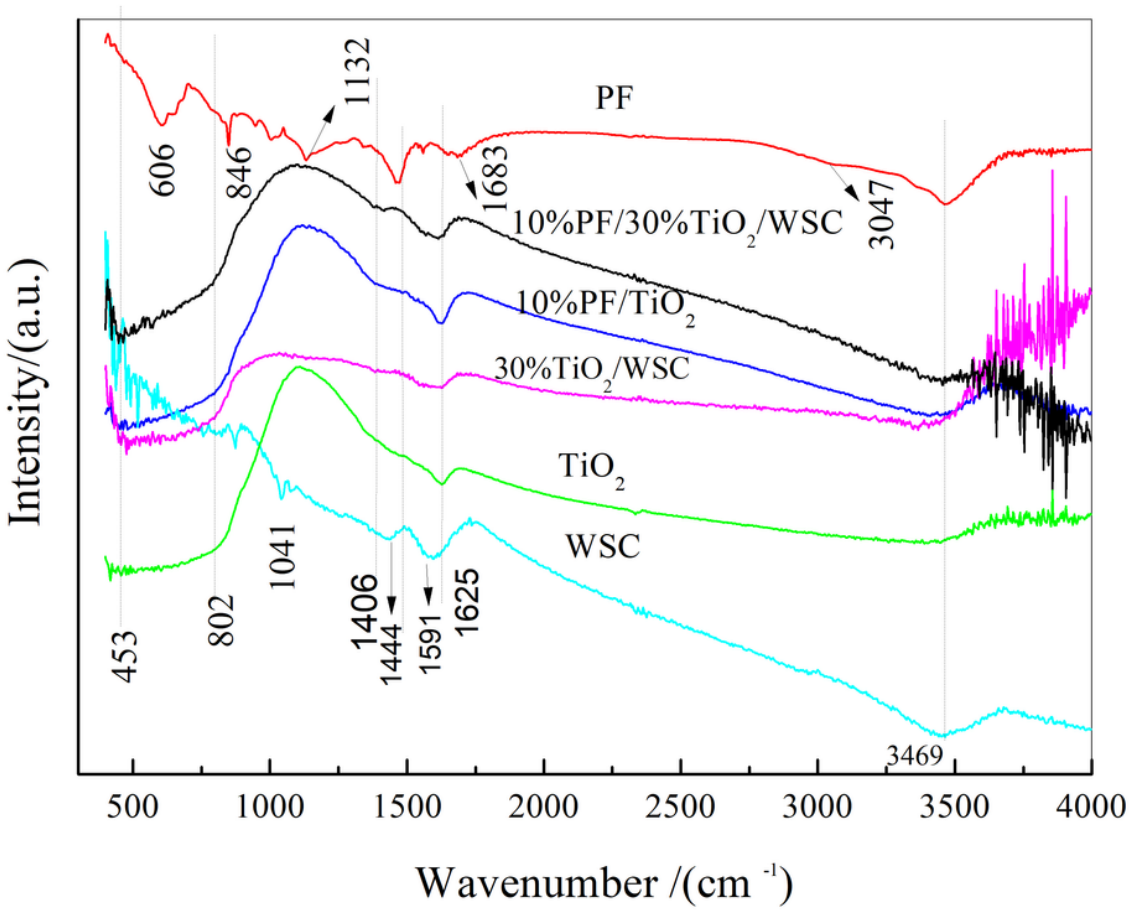

Figure 5

FT-IR spectra of different photocatalysts

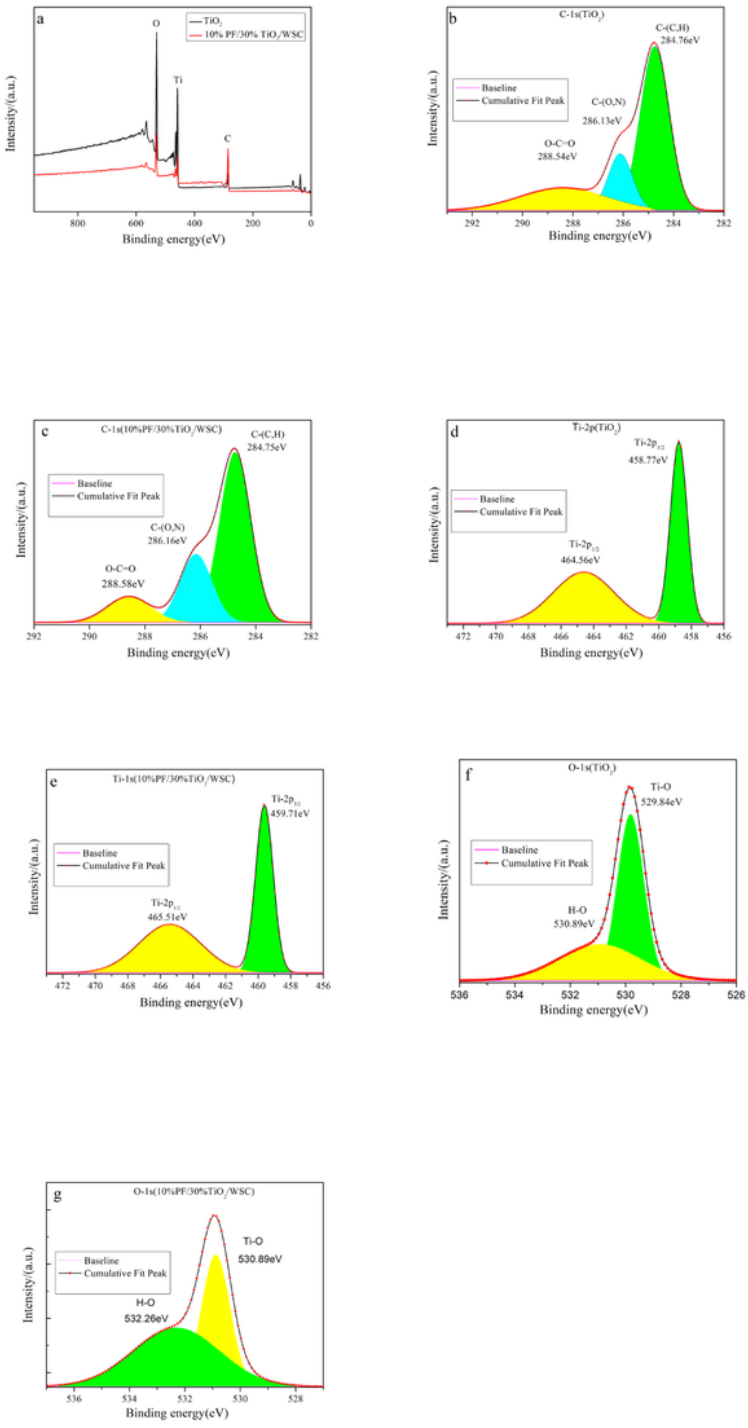

Figure 6

Legend not included with this version.

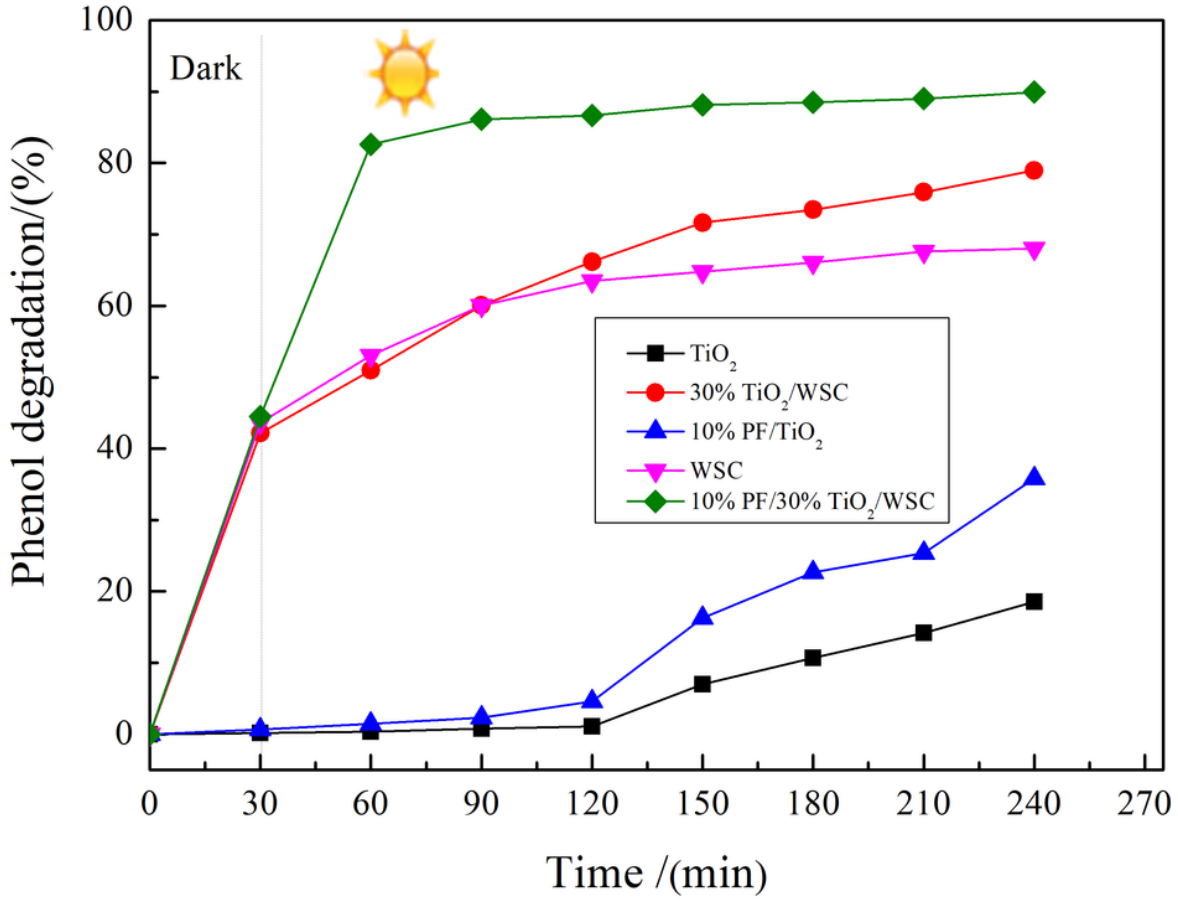

Figure 7

Combined adsorptive and photocatalytic phenol over different photocatalysts

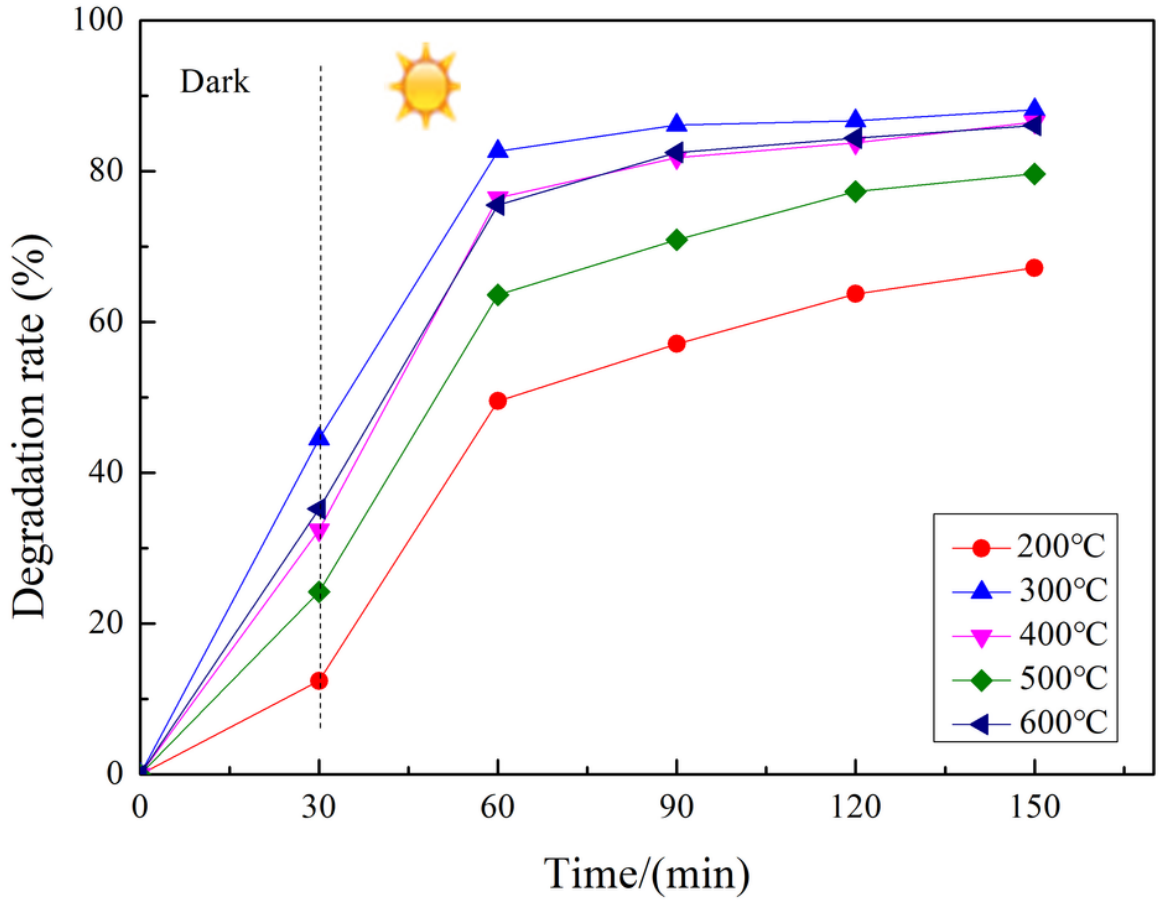

Figure 8

Legend not included with this version.

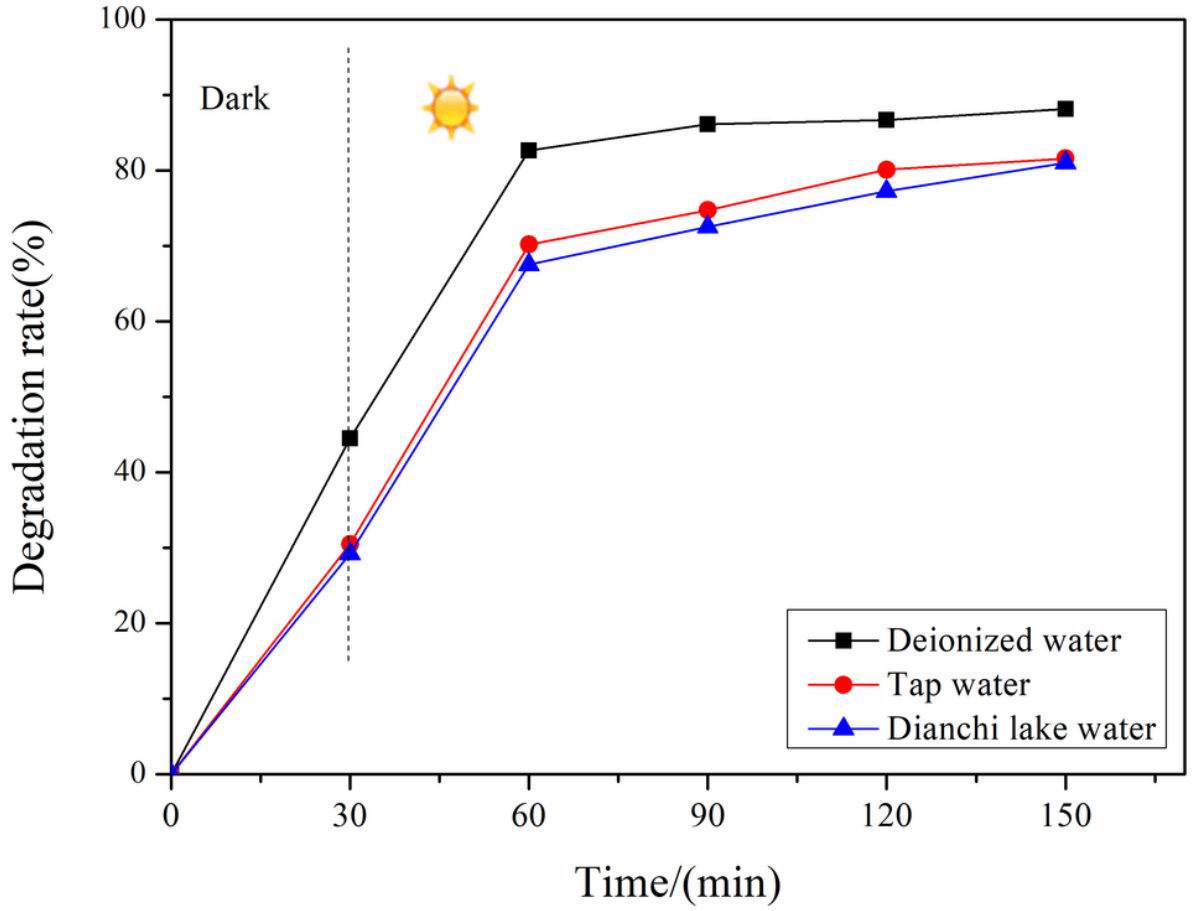

Figure 9

The influence of water source on the degradation of phenol by 10%PF/30%TiO_2/WSC

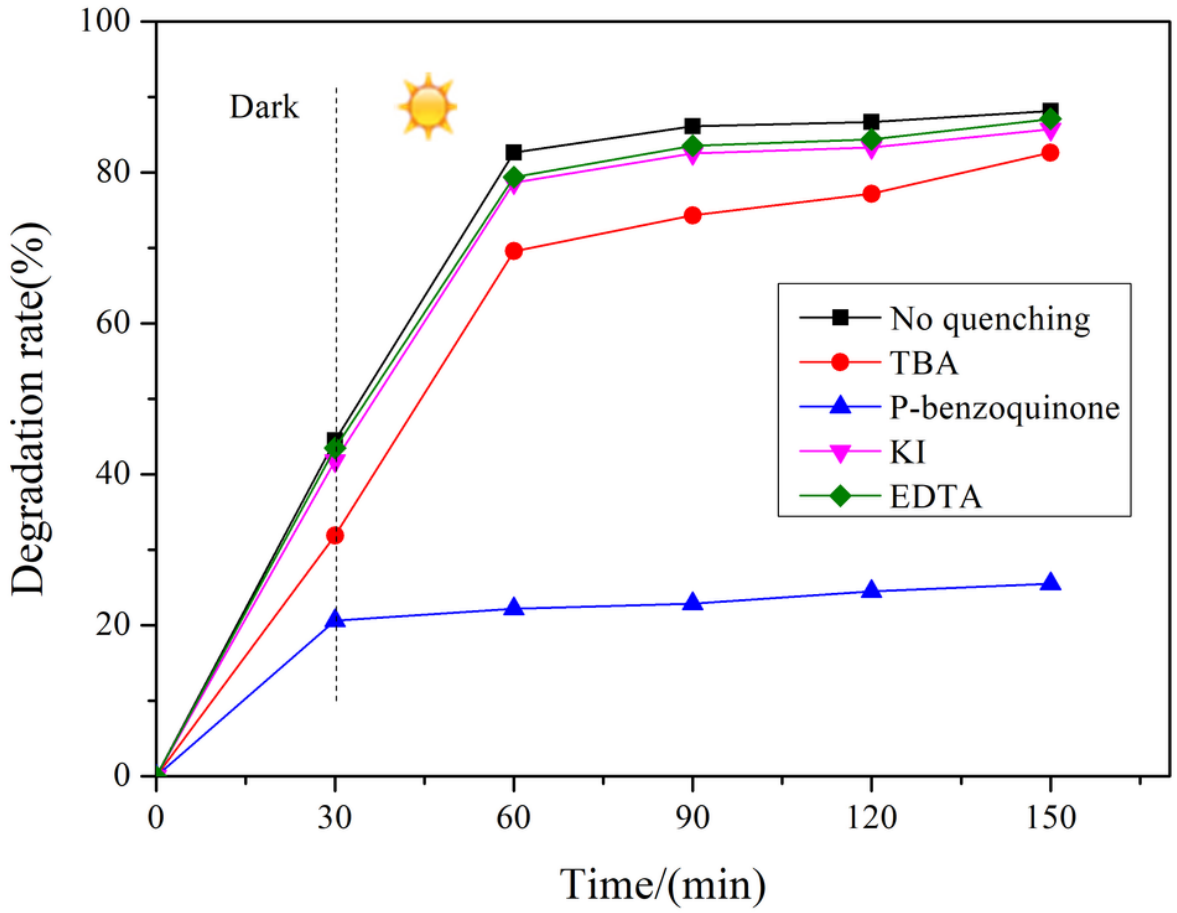

Figure 10

Trapping experiments over 10%PF/30%/TiO_2/WSC for phenol degradation

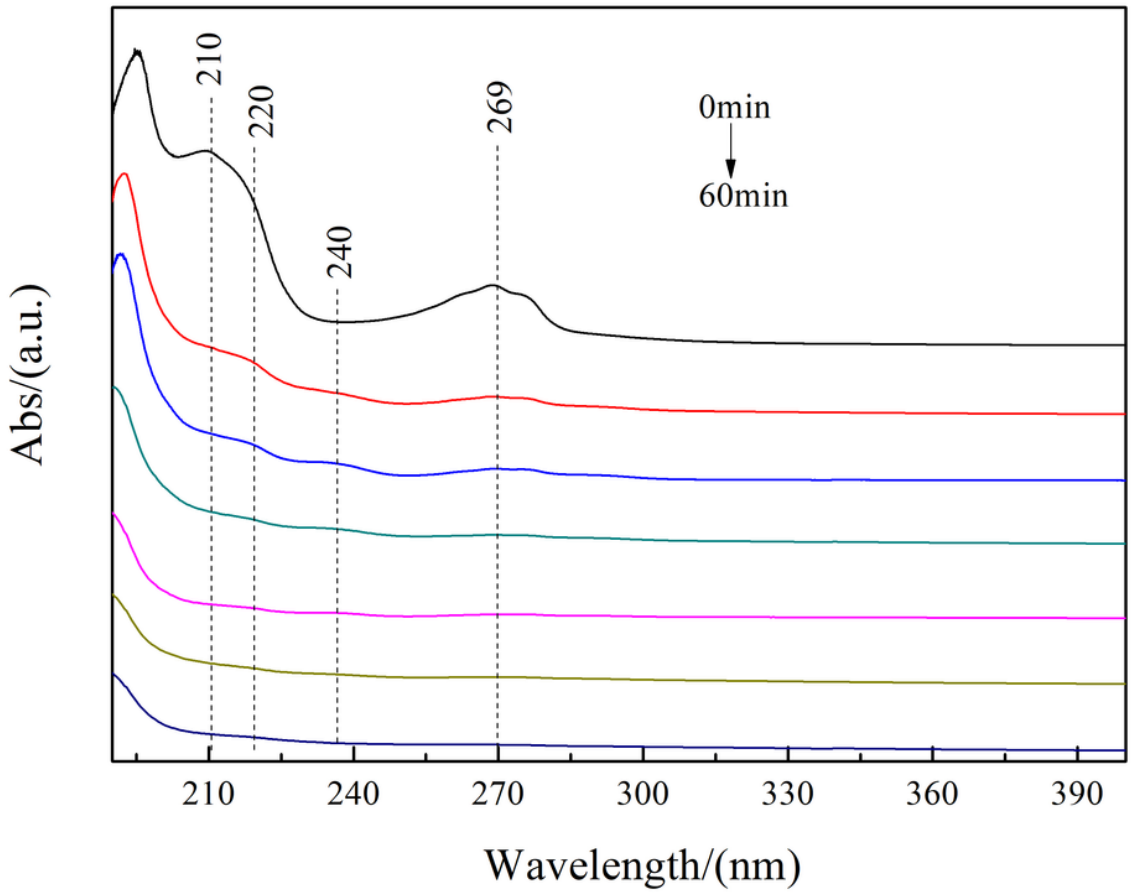

Figure 11

Legend not included with this version.

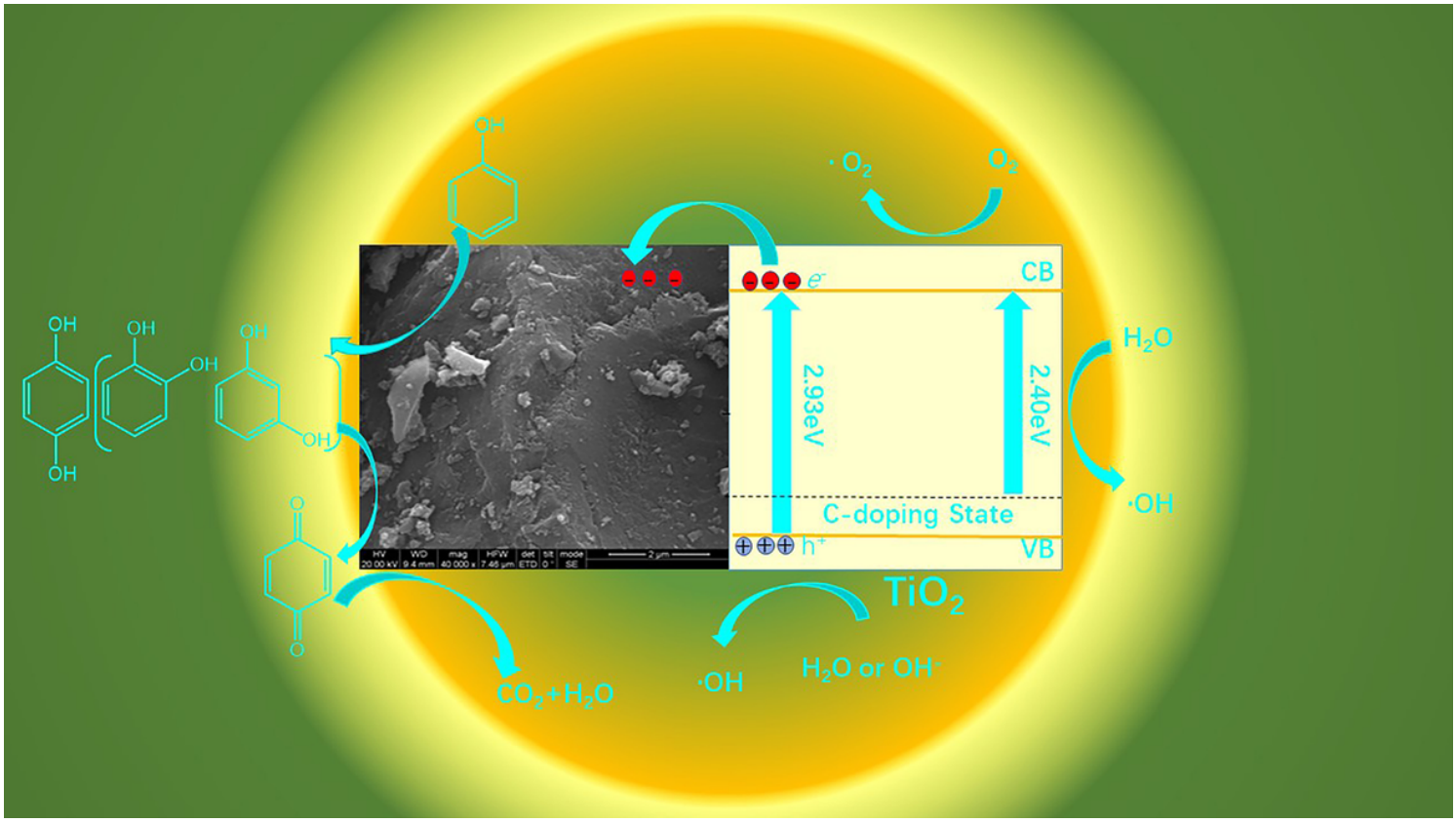

Figure 12

Mechanism model of composite photocatalyst degradation of phenol